Received <day> <Month>, <year>; | Revised <day> <Month>, <year>; | Accepted <day> <Month>, <year>

DOI: xxx/xxxx

ARTICLE TYPE

Stationary Localised Patterns for Two Types of Predator and Prey Models.

Fahad Al Saadi*[1,2] | Annette Worthy[3] | Ahmed Msmali[4]

[1]Department of Engineering Mathematics, University of Bristol, Bristol, BS8 1UB, Uk
[2]Department of Systems Engineering, Military Technological College, Muscat, Oman
[3]School of Mathematics, University of Wollongong, Wollongong, Australia
[4]Department of Mathematics, Jazan university, Jazan, Saudi Arabia

Correspondence
*Corresponding author name, Corresponding address. Email: alsaadi23@hotmail.com

Abstract

Inquiries into biological applications using mathematical models have been extensively examined over the years[1]. However, investigations into the existence of localised structures region has been limited and, therefore, examinations into solution types and patterns formations have not been thoroughly discussed. This study will, consequently, present the existence of localised structures region and the type of pattern formations for two predator-prey models using a system of reaction-diffusion equations with dissimilar nonlinearity functional responses for each of the two models.

Linear and weakly nonlinear analysis with supporting numerical methods are the mathematical tools for the analysis. Upon applying these tool, the mathematical explorations generate a particular set of system parameter conditions for: pattern formation (spatial instability); the Belyckov-Devaney transition; the coexistent of the codimension two point and localised patterns formation. Further, the use of spectral computations and numerical simulations on each model's system of equations will expose how the Hopf bifurcation influences the localised structures region. Consequently, this influence will unveil the rise of temporally periodic localised patterns at 'certain' nearby parameter values. Finally, the numerical outcomes in two dimensional space confirms the onset of intricate spatio-temporal patterns within the conformable parameter regions within one dimensional space.

KEYWORDS:
Belyakov-Devaney transition, Homoclinic snaking, Localised patterns, Weakly nonlinear stability analysis

1 | INTRODUCTION

The dynamic relationships between species and their complex properties are at the heart of many ecological and biological processes[2]. Due to their universal existence and importance within the biological and physical world, a popular dynamical inter-species relationship is between a predator and its prey. Hence, investigations into predator-prey interactions and mathematical models are dominated in both ecology and mathematical ecology[3]. Predator-prey models may appear to be mathematically simple at first sight but, in fact, are often challenging and complicated. Seeding from the Lokta-Voltera model of a predator-prey model[4,5], extensive research has been achieved reviewing, altering and improving the basic system of equations see for[6,7] over view. These equations have been utilised in other areas such as: climate change[8], parasite-host interactions[9], business-cycle fluctuations[10] and interactions between police and driver[11].

Pattern formation phenomenon is a fundamental topic in biological processes and many other scientific fields of nonlinear sciences, for instance: optics[12], dip-coating of material[13] and magnetic fluid[14]. This phenomenon is a consequence of the intersection between diffusion and reaction kinetics that leads to self-organised processes[1]. In fact, it was Turing who initially proposed that the generation of pattern formations is attained via a stable uniform distribution of reacting components in the absence of diffusion but may become unstable when diffusion is considered[15]. Theoretically, many researchers have developed a considerable number of nonlinear reaction-diffusion equations to model and analyse spatio-temporal predator-prey type dynamics. These models normally include a functional response so as to mimic the density interaction between the predator and its prey. Some of these responses and examples of their application are: the Leslie-Gower[16]; the Beddington-DeAngelis[17]; the Holling type models[18,19,20], as well as, the Ivlev and ratio-dependent responses[21,22].

This article is inspired by the latest interest in the existence of localised patterns in models that use nonlinear reaction-diffusion partial differential equations - see[23,24] for reviews. These patterns are a result from the bistability between the homogeneous steady state and the spatially periodic patterned state[25,24,26]. Such localised patterns also have been revealed in various studies such as: fluid dynamics[27]; optics[28]; biology[25,24] and ecology[29,30] . Consequently, we are motivated to study predator-prey type models where the onset of localised patterns may be discovered. Importantly, we will concentrate on localised patterns with temporal periodicity that may be driven by the Hopf bifurcation. In this paper, the interpretation is also in the same spirit as recent relevant bifurcation investigations in[31].

The rest of the paper is organised as follows. In Section 2, we carry out preliminary analysis using a generalised predator-prey model that employs a system of reaction-diffusion equations in one or two spatial dimensions (i.e. $1D$ or $2D$). Specifically, through the employment of linear stability analysis, the necessary conditions under which spatial instability occurs along with the Hopf bifurcation are determined. Further, through the use of weakly nonlinear analysis, an analytical expression for the codimension two parameter point is ascertained. This is where the spatial instability curve bifurcates from a subcritical to a supercritical bifurcation. Section 3 contains the first of two selected predator-prey models where the nonlinearity is the Ivlev functional response. This section establish the existence of a localised structures region. Also, by using specific parameter values of the model, the bifurcation diagram in a two parameter space is produced. Further, through simulations and numerical continuation results of stable localised patterns is generated in $1D$ and $2D$. For the second example, in Section 4, the Holling II functional response is used and the resulting system model is analysed. This particular example support the Ivlev system qualitatively results. Finally, the concluding remarks are given in Section 5.

2 | PRELIMINARIES

Following the works of[32] and[31], the aim of this section is to set up the preliminary mathematical tools for the following sections to demonstrate the existence of a localised structures region in two different predator-prey models. As well as, set up the parameter conditions for a general model.

Consider the following general dimensionless nonlinear reaction-diffusion coupled system of partial differential equations (PDEs) that is in either $1D$ or $2D$ spatial dimensions:

$$u_t = \epsilon^2 \nabla^2 u + f(u, v), \tag{1a}$$

$$v_t = \nabla^2 v + g(u, v) \tag{1b}$$

where u, v are the dependent population variables in both time, t and the spatial co-ordinates (x, y) where $x, y \in (-L, L)$. Here, the Laplacian operator in $2D$ space is given by $\nabla^2 = \frac{\partial}{\partial x^2} + \frac{\partial}{\partial y^2}$ while $f(u, v)$ and $g(u, v)$ are generic functions that will be specified in later sections. Also, ϵ is the diffusion ratio that is determined by the ratio of diffusion rates for u divided by v. It will be assumed that $\epsilon \ll 1$ and, therefore, the population of v is more mobile than that of u. The system of equations is subject to homogeneous Neumann boundary condition at each of the boundaries i.e. $x = \pm L$ and $y = \pm L$ for some $L \gg 1$.

2.1 | Homogeneous steady states

To achieve some dynamical insight into solution behaviour, the initial analysis will be based on the $1D$ version of (1). Hence, we start by determining the homogeneous steady states through setting the spatial and time derivatives to be zero. If it exists,

the nonzero homogeneous coexistence steady state will be written as:

$$\mathbf{S}_+ = (u^*, v^*) \tag{2}$$

which is of interest in this paper only. In the resulting the analysis, $\mathbf{S}_+$ will generate conditions on some of the system's constant parameters so as to be physically meaningful.

2.2 | Linear stability analysis

The stability analysis outlined in[33] is now implemented. Here it is assumed that the solution for (1) is near (2). Hence, we will determine a solution by using the following transformation:

$$(u, v)^T = (u^*, v^*)^T + (U, V)^T. \tag{3}$$

Hence, upon the substitution of (3) into (1) we obtain the following nonlinear system of PDEs:

$$(U, V)_t^T = \left[J|_{\mathbf{S}_+} + D\partial_{xx}\right](U, V)^T + (U, V)^T NL(U, V)|_{\mathbf{S}_+} \tag{4}$$

where $\left[J|_{\mathbf{S}_+} + D\partial_{xx}\right]$ represents the linear operator of (1) with J being the Jacobian matrix evaluated at (2), D is a diagonal matrix that accounts for the diffusion coefficients associated with the second order spatial derivatives, $NL(U, V)|_{\mathbf{S}_+}$ is a scalar quantity that reflects the nonlinear terms in (1) after using the translation in (3).

To determine a solution pattern of the linearised form of (4), we neglect the nonlinear terms that are exhibited in this equation. We consequently, use an ansatz solution of the form:

$$(U, V)^T = (a, b)^T e^{ikx+\lambda t} \tag{5}$$

where the constants a, b (for $||(a, b)|| \ll 1$) are regarded as the real-valued amplitudes of the periodic solution for (U, V). Here, the introduced parameters k and λ are the wave number and the growth factor or temporal eigenvalue, respectively, and i is the usual imaginary unit.

Upon substitution of (5) into the linear form of (4) generates the dispersion equation that can be rearranged into the form:

$$\lambda(k) = \frac{T_k \pm \sqrt{T_k^2 - 4D_k}}{2} \tag{6}$$

where T_k, D_k are, respectively, the trace and determinant of the matrix $\left[J|_{\mathbf{S}_+} + D\partial_{xx}\right]$. It is noted here that the expression for λ in (6) indicates that there is a spectrum of eigenvalues which are dependent on the wave number k.

Analysing the stability of the homogeneous steady state solution for the linearised form of (4), it is clear that this solution will be stable (unstable) whenever the $\Re(\lambda) < 0$ ($\Re(\lambda) > 0$).

Further, we shall consider the existence of two kinds of bifurcation that leads to symmetry-breaking. These being: the time independent Hopf bifurcation and, the spatial instability (Turing instability) bifurcation. Firstly, the Hopf bifurcation breaks the temporal symmetry of (1) to give oscillations that are stationary in space but periodic in time. This type of bifurcation exists when

$$\Im(\lambda(k)) \neq 0, \quad \Re(\lambda(k)) = 0, \quad k = 0. \tag{7}$$

Implementing the conditions in (7) on (6), we can obtain an expression for the critical value of the Hopf bifurcation. Note that $\mathbf{S}_+$ in (2) is stable to the spatially homogeneous mode $k = 0$.

The second bifurcation occurrence is the spatial instability that breaks the spatial symmetry of (1) which gives rise to periodic patterns in space but uniform in time. This bifurcation occurs whenever the following critical conditions are satisfied[33]:

$$\Re(\lambda(k_c)) = 0 \quad \text{and} \quad \Re(\partial_k \lambda(k)|_{k=k_c}) = 0 \tag{8}$$

where k_c is the critical value for the wave number k. Applying (8) to (6), we can obtain two expressions which are: the critical bifurcation curve for the spatial instability of the system (1); and, its critical wave number value (k_c). As claimed in[25], the spatial instability conditions in (8) can be explained as a Hamiltonian-Hopf bifurcation in terms of the spatial dynamics when the steady state problem is extended to an infinite domain. Consequently, the spatial variable x is regarded to be time-like. Hence, we can assume that the pattern solutions are independent of time and, therefore, the solution for (4) can be written in the form:

$$(U, V)^T = \left(Ae^{ik_c x} + \bar{A}e^{ik_c x}\right)\Phi^T \tag{9}$$

where Φ is the vector obtained from the Ker $\left[J|_{\mathbf{S}_+} + D\partial_{xx}\right]|_c$ in (4) and A is the constant amplitude of the pattern.

Furthermore, from the linear stability analysis, another interesting transition curve occurs when the spatial eigenvalues change from purely real to complex conjugates. This transition boundary is called the Belyckov-Devaney (BD) curve[34,35,36] whereby the solution of the localised patterns changes from having a monotonic decaying tail to an oscillatory one.

2.3 | Weakly nonlinear analysis

The physical parameters that govern the system's solution behaviour are inter-dispersed within the functions f and g. These functions are depicted in (1) and, hence, (4). By selecting two of these parameters, we obtain an analytical expression for a codimension two parameter point whereby the the critical curve of spatial instability changes from a subcritical to a supercritical bifurcation. This is achieved by undertaking the normal form analysis detailed in[35] and used in[32,37]. In this section for simplicity, we will only give some of the prominent details for the weakly nonlinear analysis along with relevant explanations.

Accordingly, weakly nonlinear analysis is applied to (4) with the aim to determine the amplitude equation arising from any spatial instability. Thus, we follow[32] to determine the coefficients of the normal form. That is, we assume that $A = A(t)$ in (9) and we seek the amplitude and solution of (4) to be of the form:

$$\partial_t A \;=\; \sum_{i=1}^{\infty} R^{(i)}(A), \tag{10a}$$

$$(U, V)^T \;=\; \sum_{i=1}^{\infty} \mathbf{P}^{(i)}(A, x) \tag{10b}$$

where $R^{(i)}(A)$ and $\mathbf{P}^{(i)}(A(t), x)$ for $i = 1, 2, 3, \ldots$ are functions that represent the decreasing orders of magnitude in A.

From here the mathematical details are standard but lengthy and hence we present only the essential equations in this procedure. Consequently, (4) can be solved now for each order in A. For example, the first-order coupled equation between $R^1(A)$ and $P^1(A, x)$ is given by:

$$\partial_A \mathbf{P}^{(1)}(A, x)\partial_t R^{(1)}(A) \;+\; c.c. \;=\; \left[J|_{\mathbf{S}_+} + D\partial_{xx}\right]\mathbf{P}^{(1)}(A, x) \tag{11}$$

where $c.c.$ means the complex conjugate of $\partial_A \mathbf{P}^{(1)}(A)\partial_t R^{(1)}(A)$. This order corresponds to the linear approximation of (4) which means that amplitude is a constant and, therefore, $\partial_t R^{(1)}(A) = 0$. Hence, the solution for this order is given by (9). As we are interested in obtaining the pattern solution, an analytical expression for A to the third order is generated from (10) (see[32] for more detail). This equation being:

$$\partial_t A \;=\; \rho C_1 A \;+\; C_3 A|A|^2 \;+\; O(A|A|^4). \tag{12}$$

Here C_i , $i = 1, 3$ are constants that are achieved by the solvability conditions which can be represented in term of all parameters of the problems. Note that ρ is an unfolding parameter which is permitted to show a small variation around the homogeneous steady state. Once C_3 in (12) is achieved, we can then seek a change in sign of C_3 which shows where the spatial instability bifurcation changes from being subcritical to a supercritical bifurcation.

2.4 | Nonhomogeneous solution

To gain further indepth understanding of the dynamics of (1), we focus here on the time-independent solution for the $1D$ case. Consequently, the system (1) is reduced to the following coupled system of two nonlinear spatial second order differential equations (ODEs) in x.

$$\epsilon^2 \nabla^2 u + f(u, v) \;=\; 0, \tag{13a}$$

$$\nabla^2 v + g(u, v) \;=\; 0. \tag{13b}$$

Hence, we can now analyse the spatial dynamics of (1) by the adaption of the usual method of converting the system of equations in (13) into four first order nonhomogeneous nonlinear ODEs of the form:

$$\mathbf{Z}_x \;=\; \mathbf{B}(x, \mathbf{Z}) \tag{14}$$

where $\mathbf{Z}^T = (z_1, z_2, z_3, z_4)$ with $z_1 = u(x), z_2 = u_x(x), z_3 = v(x), z_4 = v_x(x)$ and $B(x, \mathbf{Z})$ is a 4×1 vector-valued function of 4 variables that is dependent on the functions f and g. It is important to note that (1) is spatially invariant under reflection

and, therefore, leads to the invariance of the dynamical system in (14). Consequently, (1) is spatially reversible - see [36,35]. The advantage of this transition is to allow the numerical continuation to be apply. This is to sight the appearance of localised structures region and trace the different types of localised patterns with the variation of the system parameters. Further, it permits the set up of a relationship between the solutions of the stationary equation (13) and the dynamical system found in (14). In contrast, there are disadvantages of reducing the system to nonlinear ODEs. For instance, no information is achieved concerning the system's temporal stability and, consequently, we need to study the full system of PDEs using numerical simulations.

Here, the continuation package AUTO is used so as to compute the localised patterns. As result of the symmetry in the spatial system, the half domain $[0, L]$ for $L \gg 1$ is considered by applying the homogeneous Neumann boundary conditions to solve the steady-state problem of the system (1). Generally, when displaying a bifurcation diagram in a single parameter, we utilise the default vector L_2norm in AUTO:

$$L_2\text{norm} = \sqrt{\frac{1}{L}\int_0^L \left(u^2(x) + u_x^2(x) + v^2(x) + v_x^2(x)\right) dx}\,. \tag{15}$$

The full PDE system's numerical solution is achieved through explicit finite difference method with Neumann boundary conditions where the time and space increments were chosen as $dt = 0.001$ and $dx = 0.05$, respectively. Furthermore, to determine the solution stability, we adopt the finite difference approximation method to linearised (1) about the nonhomogeneous steady state. Also, by using Matlab, the spectrum of eigenvalues for the linear operator is acquired through the discretisation of the nonhomogeneous solution of (1).

In the next two sections, we implement the above methodology so as to investigate the existence of localised structures region in two predator-prey type models that are based on a system of reaction-diffusion equations. Topical predator-prey type functional responses used by ecologists and mathematicians in this type of system of equations are the Ivlev and Holling II responses both of which will be considered below.

3 | THE IVLEV MODEL

Based on field data, Holling [38] suggested that the predator-prey functional response or their interaction should be a function that is monotonically increasing and uniformly bounded. Ivlev [39] suggested a functional response of the form $b(1 - e^{-au})$ where a, b are constants and, as a consequence, this response is called the Ivlev functional response or model. The Ivlev model has been used in a variety of predator-prey applications [40,41,42,43,44,45,46] and thus of a great interest to both mathematicians and ecologists. Specifically, some ecological applications using the Ivlev-type model are: aquatic ecosystems, such as, plankton population dynamics [47]; the interactions between a host and a parasite [48] and integrated pest control management [49]. Mathematical interest in using the Ivlev model can be found in such work as: [50,51,52] who analysed the predator-prey dynamics; investigations by [44,41] who explored the occurrence and uniqueness of the limit cycle; the stability and the Hopf bifurcation was considered in [53] while [54,55] reviewed the existence and stability conditions of a positive periodic solution. Further, the spatial patterns using the Ivlev model was shown in [46,21].

The following work uses the Ivlev functional response in a predator-prey reaction-diffusion coupled system of nonlinear PDEs. This system of equations will be referred to as the Ivlev system and, from there, we will investigate the existence of localised patterns. Thus, the given Ivlev system in either $1D$ or $2D$ spatial dimensions is given as:

$$u_t = f(u, v) + \epsilon^2\nabla^2 u = u(1 - u) - v(1 - e^{-\alpha u}) + \epsilon^2\nabla^2 u, \tag{16a}$$

$$v_t = g(u, v) + \nabla^2 v = \delta\beta v(1 - e^{-\alpha u}) - \beta v + \nabla^2 v \tag{16b}$$

for $x, y \in (-L, L)$, subject to the homogeneous Neumann boundary condition at each of the boundaries ie $x = \pm L$ and $y = \pm L$ for some $L \gg 1$.

Respectively in (16), u and v represent the prey and predator population densities. The parameter α is the efficiency of predator capture of prey, β is the death rate of the predator and δ is a measured of the conversion rate of prey captured by the predator.

From Section 2.1, a straightforward calculation shows that (16) has three homogeneous equilibrium states. These are: the prey and predator population extinctions $(0,0)$ states; the free predator $(1,0)$ state, and the coexistence $\mathbf{S}_+ = (u^*, v^*)$ state where

$$u^* = -\frac{\xi}{\alpha}, \quad v^* = -\frac{\xi\delta\ (\xi+\alpha)}{\alpha^2} \quad \text{where} \quad \xi = \ln\left(\frac{\delta-1}{\delta}\right). \tag{17}$$

The positive coexistent steady state, as described in (17), exists under the following parameter conditions:

$$\delta > 1 \quad \text{and} \quad \alpha > 0 > \xi.$$

3.1 | Bifurcation conditions with its geometry

The standard linear stability analysis (as per[33]) is implemented on (4) and is generically described in Section 2.2. On comparison of the particular Ivlev system in (16) with the more generic predator-prey model found in (1), it can be seen that the functions $f(u,v)$ and $g(u,v)$ are specified but basically they are the same equations. Therefore, for clarity and brevity the general equations and theory that is given in Section 2 will be referred to and (when required) specific equations relating to (16) will be given. Hence, by using the coexistent steady state given by (17), the ansatz solution (5) is imposed on (4).

Thus, after neglecting the nonlinear terms of (4), the specific dispersion relation for (6) is obtained and is reworked to be written as:

$$\lambda^2 - T_k\lambda + D_k = 0 \tag{18}$$

where

$$T_k = \frac{(\delta-1)\,\xi^2 + (2+(\delta-1)\,\alpha)\,\xi - \left(-1+\left(\epsilon^2+1\right)k^2\right)\alpha}{\alpha}$$

and

$$D_k = \frac{-(\delta-1)\left(k^2+\beta\right)\xi^2 + \left(-(\delta-1)\left(k^2+\beta\right)\alpha - 2\,k^2\right)\xi + \left(\epsilon^2k^4 - k^2\right)\alpha}{\alpha}.$$

By using the details in (18), we can now determine the stability of the coexistence homogeneous steady state for (16). As discussed in Section 2.2, this state is stable whenever the $\Re(\lambda) < 0$. Hence, implementing (7) and using the details given in (18), the critical value (α_H) for the Hopf bifurcation is:

$$\alpha_H = \frac{((1-\delta)\,\xi - 2)\,\xi}{1+(\delta-1)\,\xi}. \tag{20}$$

Applying the conditions for spatial instability found in (8), we gain a critical bifurcation expression for the spatial instability and the critical value for the wave number (k_c) as follows:

$$(\delta-1)\,\xi^2 + (2+(\delta-1)\,\alpha)\,\xi + \alpha = 2\,\epsilon\,\sqrt{-\alpha\,\xi\,\beta\ (\delta-1)\,(\xi+\alpha)}, \tag{21a}$$

$$k_c^2 = \frac{(\delta-1)\,\xi^2 + (2+(\delta-1)\,\alpha)\,\xi + \alpha}{2\alpha\,\epsilon^2}\ . \tag{21b}$$

Further, the BD transition curve is found to satisfies the following equation:

$$(\delta-1)\,\xi^2 + (2+(\delta-1)\,\alpha)\,\xi + \alpha = -2\,\epsilon\,\sqrt{-\alpha\,\xi\,\beta\ (\delta-1)\,(\xi+\alpha)}. \tag{22}$$

Figure 1 a displays various dispersion curves for $\Re(\lambda)$ versus k, whereby pre-selected parameters values of β, δ and ϵ are substituted into (18) and α is allowed to vary. This figure identifies three different scenarios of spatial instability for (16) such that: $k > k_c$ is unstable (red solid curve); $k = k_c$ is the critical value of spatial instability (black dot curve) and $k < k_c$ is stable (blue dashed curve).

Hereafter, we will fix the parameter values of δ and ϵ to be 1.1 and 0.06, respectively. Hence, on application of weakly nonlinear analysis found in Section 2.3 on (16), the algebraic expression for C_3 is obtained. Consequently, Figure 1 b displays the values of C_3 as a function of the single variable α by noting that $\beta = \beta(\alpha)$. The green circle indicated on the plot depicts the point where C_3 changes sign, that is, at $\alpha = 6.034$. This particular point is called the codimension two point (or the specific (α,β) point when $C_3 = 0$) and indicates where the spatial instability bifurcation transitions from being a subcritical (red curve) to supercritical (black curve). That is, it means that C_3 is negative (positive) for $\alpha < 6.034$ ($\alpha > 6.034$) in the given figure. Thus, due to the change in sign of C_3, the bio-stability between the homogeneous steady state and the pattern state emerges. This indicates where the localised patterns may be born.

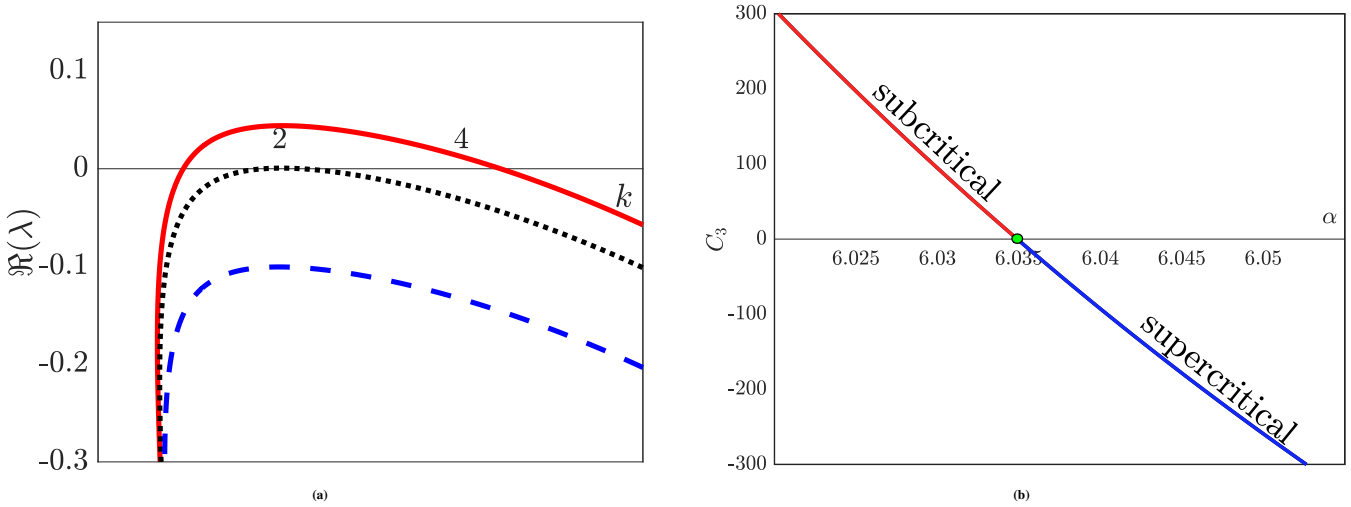

FIGURE 1 (Colour version online.) (a) Dispersion relation curves for (16) using $\beta = 0.426$, $\delta = 1.1$, $\epsilon = 0.06$, and three different values of α . The solid red line indicates the case of spatial instability when $(k > k_c)$ using $\alpha = 6.15$, the dotted black line represents the case of the double zero root when $(k = k_c)$ using $\alpha = 5.78$ and the dashed blue line corresponds to the stable solution when $k < k_c$ using $\alpha = 5.07$. (b) A plot of $C_3 = C_3(\alpha)$ for fixed $\delta = 1.1$ and $\epsilon = 0.06$.

3.2 | The bifurcation diagram and localised structures solution patterns

For the Ivlev system found in (16), the (α, β)-plane in Figure 2 displays the system's two parameter bifurcation diagram. This diagram consists of several boundaries which identifies particular solution characteristics or behaviours that have been generated using Section 3.1. The pink curve in this diagram indicates the spatial instability boundary that was obtain from (21). For the coexistent steady state, this curve splits the bifurcation diagram into two spatial stability regions which are unstable (stable) to the right (left) of the curve. Additionally, this figure includes the Hopf bifurcation boundary (red dashed line) which is given in (20) and is β independent. This line adds intricacies to the solution behaviour of (16). That is, independent of the spatial instability curve, the Hopf bifurcation line splits the bifurcation diagram into two regions and, therefore, there are formations of two different temporal solution stability characteristics. These stability are characterised by either being stable (unstable) to the left (right) of this line. An affect of the Hopf bifurcation line is that the region on the right has a global oscillatory mode.

Further in Figure 2 , using the spatial instability curve from (21a), the codimension two point (α, β) (green dot) is evaluated to be (6.034, 1.773). Therefore, the spatial instability bifurcation is supercritical for $\beta > 1.773$ when α increases and is subcritical for $\beta < 1.773$ when α decreases. As a result, the localised structures region is established from this codimension two point.

Additionally, using the numerical continuation package AUTO, Figure 2 includes the bifurcation (black) curve that envelopes the localised structures (yellow) region (with $\beta \geq 0$). Further, generated from (22), it can be seen that this region is divided by the BD transition (blue) curve to form two localised structures sub-regions. The sub-region to the right of the BD curve is called the snaking region where the solution's spatial eigenvalues are complex conjugates with the tail of the localised patterns decaying oscillatory. On the other hand, the left sub-region of this curve is called a single hole region where the solution has purely real spatial eigenvalues with the tail of the localised patterns is decaying monotonically.

Hence, the leading spatial eigenvalues of purely spatial part of (16) can be summarised as follows:

Region	Spatial eigenvalues
Right of BD curve	Purely real
Between BD curve and spatial instability curve	Complex conjugate
Right of spatial instability curve	Purely imaginary

TABLE 1 The configuration of the spatial eigenvalues of the purely spatial system of (16).

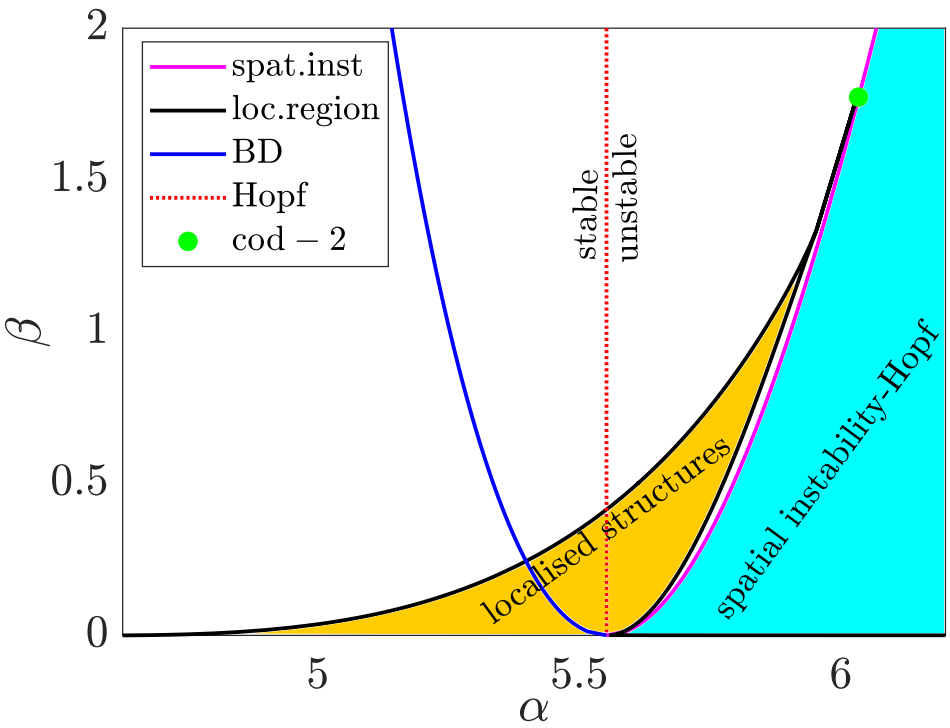

FIGURE 2 (Colour version online.) The Ivlev system (α, β) bifurcation diagram with fixed parameter values for $\epsilon = 0.06$ and $\delta = 1.1$. The blue region identifies the spatial instability (spat.inst) region and the yellow region is the localised structures region (loc.region) where the localized patterns exist. The green dot indicates where the codimension two point (cof-2) lies.

The previous sections focused on the qualitative analysis to determine solution behaviour to the Ivlev system. In the next section, the centre of attention will be on the further development of solution behaviour by numerical means.

3.3 | Numerical continuation

From here, the adopted procedure as given in Section 2.4 is to transform (16) into four first-order nonlinear ODEs as indicated by (14), where

$$\mathbf{B}(x, \mathbf{Z}) = \begin{pmatrix} z_2 \\ z_3(1 - e^{-\alpha z_1}) - z_1(1 - z_1) \\ z_4 \\ \beta z_3 - \delta\beta z_3(1 - e^{-\alpha z_1}) \end{pmatrix}. \tag{23}$$

Accordingly in Figure 3 , upon using (23) in (14), the one parameter continuation in α is shown against the default vector - the L_2norm. In this figure, two solution branches of the localised patterns are displayed. These branches are described as: one branch that is related to the odd number of solution holes (purple curves); and, the other that is associated with the even number of solution holes (brown curves). Consequently, these solution branches continue to undergo homoclinic snaking til infinity. However, in the finite spatial domain, this snaking process ends when the hole patterns solution fills the domain. Over the parameter range of $\alpha \in (5.53, 5.745)$, it is noted that the solution branches are convoluted due to the sequence of saddle node bifurcations that wobble backwards and forwards. This is call the snaking or pinning region[28,56,57]. These solution curves are born unstable at $\alpha = 5.745$. Consequently, at each left (right) saddle node bifurcation there is a temporal stability change whereby the solution branches of the snaking gains (loses) stability.

It is essential to emphasise that the Hopf bifurcation of the background steady state described in (17) is identified as a red dashed line in Figure 3 . This bifurcation line cuts the snaking diagram into two and thus creates the basis of another instability for the snaking branches. Therefore, all snaking branches upon achieving their stability at the left fold then simply lose their stability again at the Hopf bifurcation line. In contrast, in[31] it has been shown that localised patterns can inherit instability before the Hopf bifurcation curve.

In addition to that tracing the fold of one of these saddle node's in the two parameters space divulges that the black lines define the yellow or localised structures region in Figure 2 .

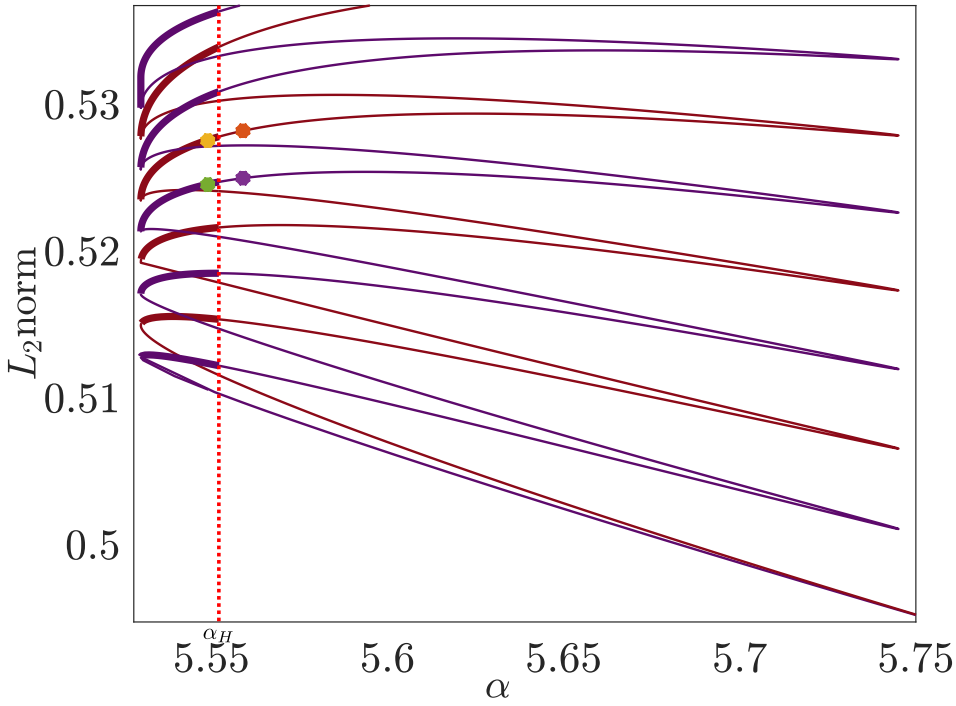

FIGURE 3 (Colour version online.) The homoclinic snaking diagram using the parameter values $\delta = 1.1$, $\epsilon = 0.06$ and $\beta = 0.3856$ while α varies. The thick (thin) line represents stable (unstable) branches. Here the purple (brown) line relates to odd (even) number of amplitude peaks. The red dashed line exhibits the Hopf bifurcation. Selected α values on the branches (coloured dots) are used to determine typical solution examples for (16) - see Figure 4 .

As described in Section 2.4, we obtain each localised hole's stability by computing the spectrum of the discretised nonhomogenous linear operator in (16). Hence, in Figure 4 , the left hand side plots depict examples of localised hole patterns from the odd (below plots) and even (top plots) branches using selected α values from the stable and unstable side the Hopf bifurcation line. Further, the right hand plots display the spectrum of leading eigenvalues that are associated to each of the localised patterns displayed in the left hand plots.

Results of the continuation from the single hole region (displayed in Figure 2) are depicted in Figure 5 . Figure 5 a shows the maximum amplitude of u (MAXu) against the continuation for β. This figure displays a single fold which is connected to two different types of branches at the saddle node bifurcation point. These branches are: stable (unstable) and are identified by a thick (thin) line. Alongside this figure (immediately on the right) are examples of solution that come from the stable (unstable) branches with their solution amplitude being large (small). Also, their corresponding leading eigenvalues for the associated solution are exhibited. Note that the instability here is the result of the growth of the amplitude with time rather than from the influence of the Hopf bifurcation. In comparison to Figure 5 a, Figure 5 b exhibits the continuation of the parameter α. It is noted that similar results are achieved whereby the unstable branch gains stability at the fold. However, in the α case, with an increase in α values, the stable branch crosses the Hopf bifurcation line and, as a result, the stable branch loses its stability.

To further study the dynamics and solution behaviour of (16), we perform direct numerical simulations on the system of equations - see Section 2.4 for further details. Notably, for the localised holes, these numerical simulations allows us to explore the nature of the Hopf (sub- or super- critical) bifurcation. Further during the investigations, we observe that the solution components of u and v have the same distribution and, therefore, we present the simulation results for the u component only.

Hence, to demonstrate the types of stability behaviour of localised patterns, a careful selection of the parameter values for α is important. From Figure 3 , two values of α are chosen from either side of the Hopf bifurcation line ($\alpha_H = 5.552$). As a result, Figure 6 represents the solution heat maps (left plots) and the associated solution time series for a single point in the spatial

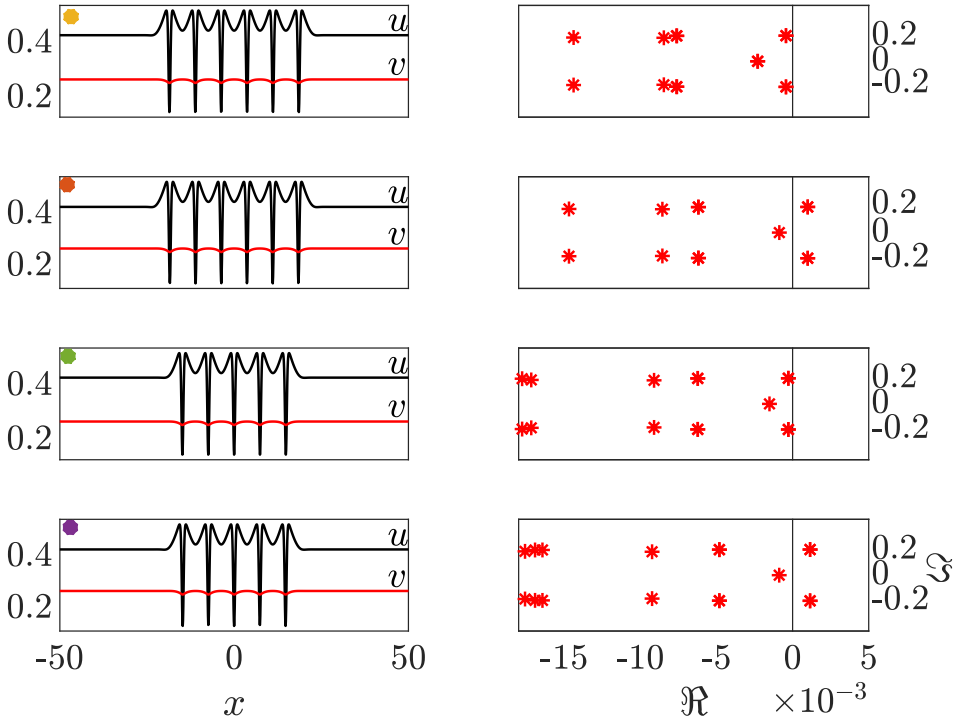

FIGURE 4 (Colour version online.) Solution profiles of (16) and their associated leading order eigenvalues corresponding to the identified dots from the snaking diagram in Figure 3 .

domain (right plots). For $\alpha = 5.545$ (a value before the Hopf line), it is evident from both the solution heat map and the time series in Figure 6 a that the solution for (16) is locally asymptotically stable. Conversely, when $\alpha = 5.65$ (a value directly after the Hopf bifurcation line), the solution to (16) evolves into a stable oscillation (see Figure 6 b). Consequently, we can remark that from the simulations that the Hopf bifurcation line is supercritical. This implies that there is a stable limit cycle just beyond the Hopf bifurcation line.

3.4 | 2D spatial simulation results

To highlight the existence of a localized structures region in higher spatial dimensions, the Ivlev predator-prey system of equations found in (16) was simulated using two spatial dimensions on a finite domain with zero flux boundary conditions. For the simulation, we considered a square domain such that $(x, y) \in [0, L]\times[0, L]$. Precisely, we adopted a finite difference method in Matlab whereby the size of the domain was chosen to be large enough so as to minimise boundary effects. Using a time step of $dt = 0.001$ and the spatial steps of $dx = dy = 0.1$, the simulation was run til the stationary state was reached or showed steady state behaviour. Moreover, the same parameter values as for the $1D$ case were kept. That is, the parameters $\delta = 1.1$ and $\epsilon = 0.06$ were fixed but α and β were allowed to vary.

For the Ivlev system given in (16), it was found that both the prey and predator have the same distribution. Therefore, the following details and numerical simulations are for the prey only. Hence, the solution heat maps are presented in Figure 7 which depicts examples of two stable localised patterns for the prey distribution. These solutions are determined by Figure 2 whereby the parameter values of: $(\alpha, \beta) = (5.5, 0.25)$ are used to represent typical values from the snaking region and $(\alpha, \beta) = (5.25, 0.1)$ are used to represent as typical values in the isolated hole region. Therefore, Figures 7 a and 7 b are the generated heat maps for the prey density in the snaking and isolated hole regions, respectively. A deduction from these figures is that the snaking region produces more but a limited amount of isolated holes. From a biological perspective, the inference from the solution heat maps in Figure 7 is that the localised holes (cold or blue spot) indicates that the prey density has been reduced by the predator while the rest of the given domain (red region) indicates that the prey is dominant and may break out.

Now, we consider the unstable region that lies within the snaking-Hopf region in Figure 2 . Importantly, this is where a careful parameter selection of (α, β) may produce a solution that exhibits a spatio-temporal behaviour that is affected by both

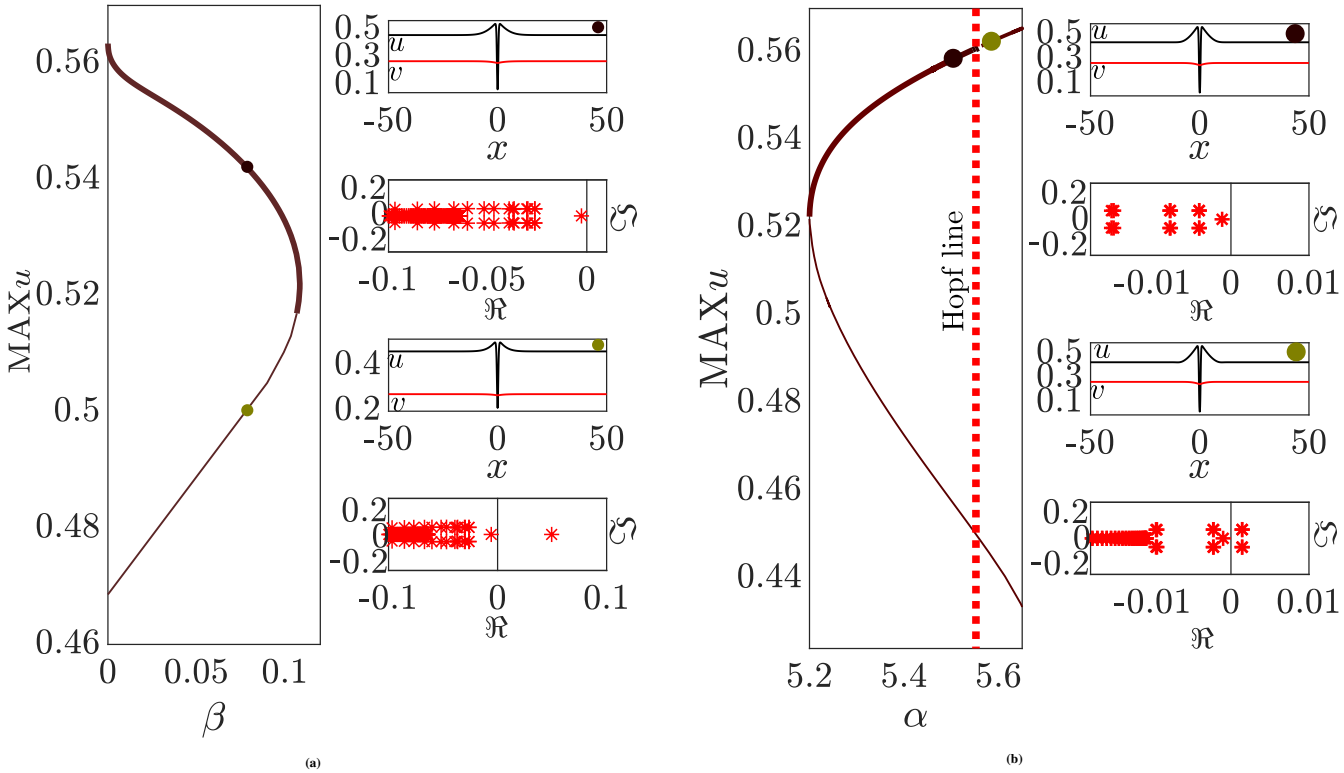

FIGURE 5 (Colour version online.) The fold of the single hole solution is presented in vector L_2-norm against the parameter α. The continuous (dashed) line indicates the stable (unstable) branch of the fold. The panels to the right correspond to the solution of the fold branches.

the Hopf bifurcation and the localised holes region. Hence, in Figure 8 , a solution heat map for the $2D$ equation found in (16) is presented to indicate this type of spatio-temporal solution behaviour that may occur within this region. Therefore, using $(\alpha, \beta) = (5.468, 0.602)$ as typical values from the snaking-Hopf region, it was found that cold spot patterns occurred but are disrupted by the unstable homogeneous solution - see in Figure 8 a. Figure 8 b displays the prey component time series at the spatially selected point $(x, y) = (25, 25)$. Due to the oscillatory nature of the time series, the solution is unstable but with finite amplitude. Thus the emerging dynamics displayed in this figure shows that through the interaction of the Hopf bifurcation and the localised holes region a mixture of stabilising spatial patterns formation but with temporal fluctuation is created. This is described as 'competing' dynamics[58,59].

4 | HOLLING II MODEL

In this section, we will present a similar system of reaction-diffusion equations as that of the Ivlev system presented in (16) except that it will have a non-identical predator-prey functional response. This new system of equations will be used so as to determine if it also exhibits a localised structures region and, if so, determine if any solutions within the region manifests a spatio-temporal behaviour. Thence, the Holling II kinetics will be used and, once results are obtained, we will make comparisons and identify similarities to that of the Ivlev predator-prey system discussed in Section 3. Consequently, to prevent mathematical repetition, reference to preliminary mathematics and analysis to determine solutions behaviour for the new equations presented below will be, where possible, referred to within Section 2 and related material from Section 3.

The Holling type II functional response[60,38] is a ratio dependent model that has the form $\frac{u}{\alpha+u}$ where α is a positive constant. Holling studied the rapacity of small mammals on the European pine sawflies, and he observed that predator rapacity rates increased with a larger prey population density and each predator increased its consumption rate when exposed to a higher prey density. This study gave impetus into the development of the Holling II functional response. This response was not only monotonically increasing, but also a uniformly bounded function in the first quadratic. In comparison, the Ivlev response is

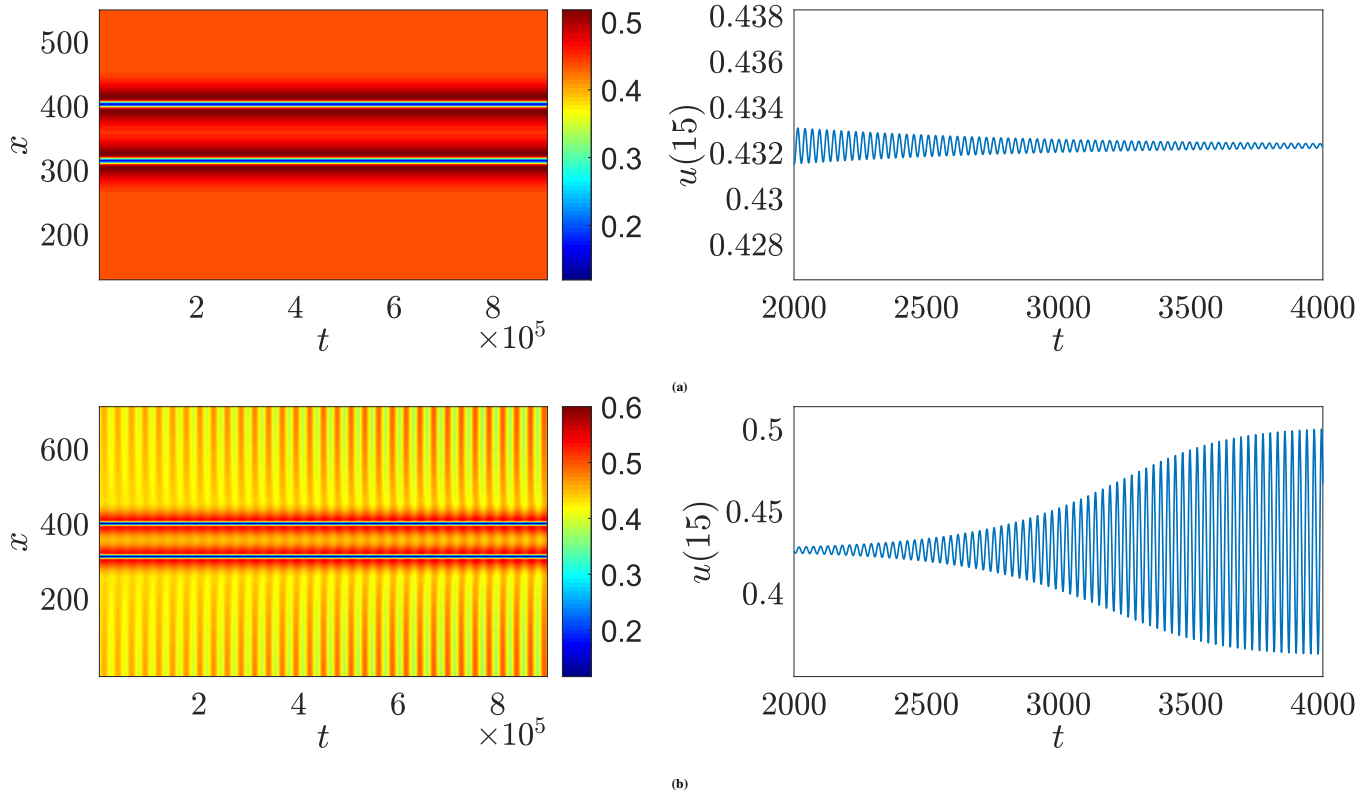

FIGURE 6 (Colour version online.) The heat map (left) and time series (right) which obtain from the numerical simulation of model (16) of the u component for two different values of α from the snaking diagram: (a) $\alpha = 5.545$, (b) $\alpha = 5.6$.

similar graphically but dissimilar in model. Thus, the Holling II response has been used in predator-prey equations and has been extensively studied in the analysis of population dynamics, see for example [18,61,62,63,64,65] and reference therein. Further, the Holling II response is equivalent to modelling of enzyme kinetics developed by Michaelis-Menten [66].

Presented below is a the predator-prey model which is a system of two reaction-diffusion equations with the Holling II response. That is,

$$u_t = u(1-u) - \frac{uv}{\alpha + u} + \epsilon^2 u_{xx}, \tag{24a}$$

$$v_t = \frac{\beta uv}{\alpha + u} - \delta v + v_{xx}, \tag{24b}$$

subject to Neumman boundary conditions. Once again, u and v are the prey and predator, respectively. All the parameters are positive where: α denotes the rate of the death of the prey by the predator; β and δ stand for the birth and death rate of the predator, respectively, and ϵ is the diffusion ratio of the prey to the predator. The system of equation (24) will be referred to as the Holling 2 system which permits many comparable properties to (16), hence, can be analysed similarly.

The Holling II system described in (24) possesses three equilibrium: $\mathbf{S}_1 = (0, 0)$, $\mathbf{S}_2 = (1, 0)$ and $\mathbf{S}_3 = (u^*, v^*)$ where

$$u^* = \frac{\delta\,\alpha}{\beta - \delta}\,, \qquad v^* = \frac{(\beta - \delta\,(\alpha+1))\,\beta\,\alpha}{(\beta-\delta)^2}\,.$$

The nontrivial or coexistent steady state ($\mathbf{S}_3$) is positive provided that $\beta > \delta$ and $\beta > \delta(1+\alpha)$. As per usual, we will focus our analysis on the coexistent steady state, $\mathbf{S}_3$.

Implementing linear stability analysis as described in Section 2.2 and around $\mathbf{S}_3$, it is found that the Hopf bifurcation occurs at the critical value $\alpha = \alpha_H$ and is given by:

$$\alpha_H = \frac{\beta - \delta}{\beta + \delta}. \tag{25}$$

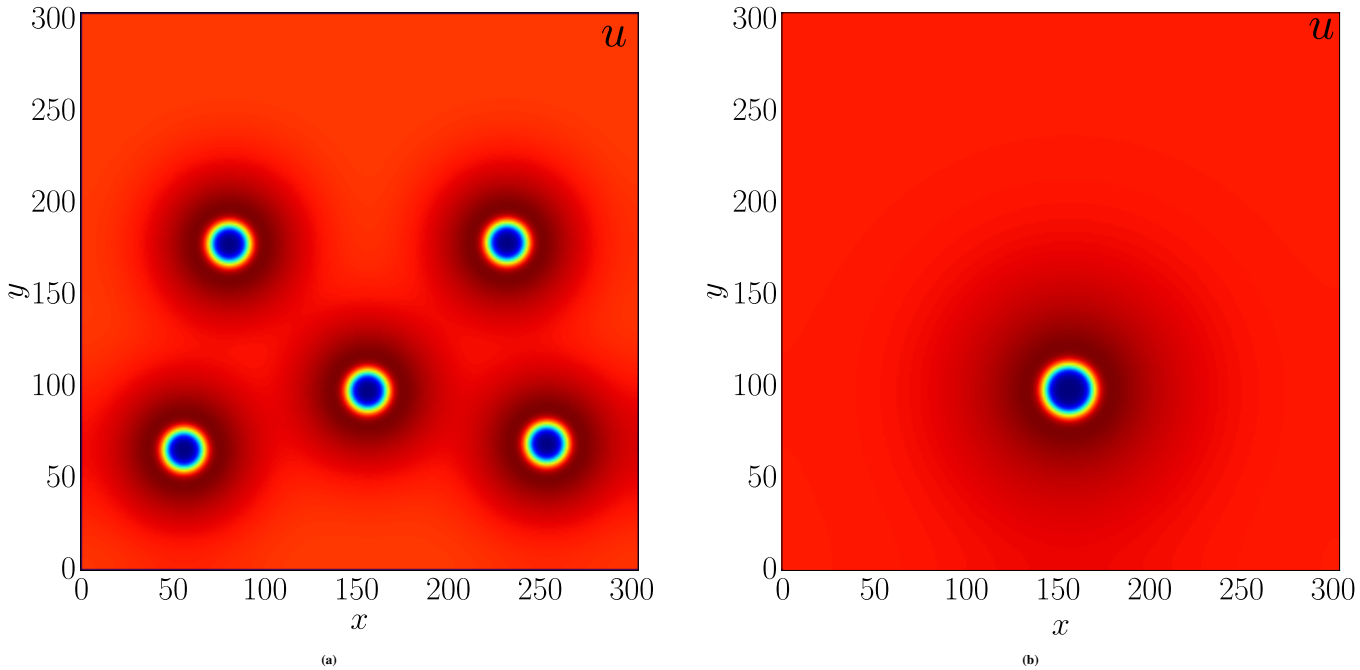

FIGURE 7 (Colour version online.) Stable $2D$ solutions for (16) from the localised structures region. (a) localised holes at $(\alpha, \beta) = (5.5, 0.25)$ and (b) single-holes at $(\alpha, \beta) = (5.25, 0.1)$.

Also, from Section 2.2, it is found that the spatial instability occurs whenever

$$\delta\ (\beta\ (-\alpha+1)-(\alpha+1)\,\delta) = -2\,\epsilon\ (\beta-\delta)\,\sqrt{\beta\,\delta\ (\beta-(\alpha+1)\,\delta)} \tag{26a}$$

with the critical wave number (k_c) as:

$$k_c^2 = -\frac{\delta\ (\beta\ (\alpha-1)+\delta\ (\alpha+1))}{2\beta\ (\beta-\delta)\,\epsilon^2}\,. \tag{26b}$$

Furthermore, the following condition that generates the BD curve from the linear stability analysis is found to be:

$$\delta\ (\beta\ (-\alpha+1)-(\alpha+1)\,\delta) = 2\,\epsilon\ (\beta-\delta)\,\sqrt{\beta\,\delta\ (\beta-(\alpha+1)\,\delta)}. \tag{27}$$

In the forgoing analysis and results, the parameter values of $\beta = 0.7$ and $\epsilon = 0.06$ are used. After applying linear and weakly nonlinear stability analysis from Sections 2.2 and 2.3, Figure 9 is created. This figure is the (α, δ)-plane bifurcation diagram and demonstrates that there are different types of regions which represent stable and unstable solution patterns. Referring to (26), the solution's spatial instability is indicated by the blue region. As well, the codimension two point $(\alpha, \delta) = (0.40789, 0.25849)$ is indicated by the blue dot. Similar to that of the Ivlev model, the localised structures (yellow) region is born from the codimension two point and is generated by using AUTO. Another similarity to that of the Ivlev model is that the localised structures region is divided into two (isolate hole and snaking) sub-regions by the BD curve described in (27). Furthermore, the Hopf bifurcation (red dashed) curve also divides the (α, δ)-plane into two sub-regions and, therefore, produces two contrasting temporal solutions. That is, the left (right) region is where the stable (unstable) temporal solution occurs. It is noted that both the Ivlev and the Holling II responses (used in (16) and (24), respectively) present similar qualitatively but not quantitative bifurcation diagrams.

Figure 10 displays the continuation bifurcation diagrams of α vs L_2norm from the snaking region (Figure 10 a) and from the isolated hole region Figure (10 b). In general, from where the primary branch is formed (in these diagrams) it is observed that for α increasing, the solution is unstable until it reaches the first fold. From here the solution becomes stable as α decreases until α_H where the solution then becomes unstable again. Also, the bifurcation diagrams includes selected values of α so as to demonstrate typical solution behaviour before (after) the Hopf bifurcation line. These are indicated by a black (green) coloured dot for α decreasing. Further, the stable (unstable) branches are represented by thick (thin) lines in these diagrams. To the right of each of the bifurcation diagrams, the inserted plots exhibit examples of stable (unstable) solutions with their largest eigenvalues.

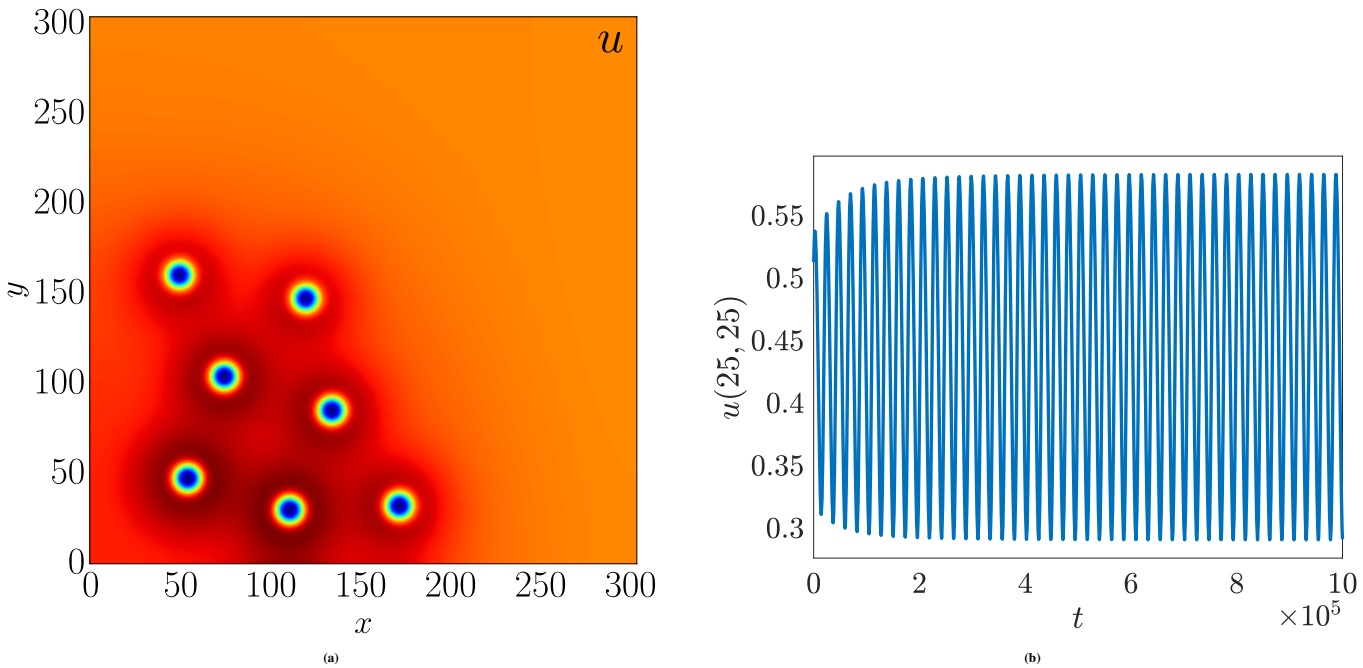

FIGURE 8 (Colour version online.) Influence of the Hopf bifurcation for the $2D$ solution using parameter values of (α, β) that are within the localised structures region. (a) solution from the unstable region of the localised localised holes at $(\alpha, \beta) = (5.768, 0.602)$. (b) The corresponding time series of the u component at the single value of the spatial domain $(x, y) = (25, 25)$.

It is observed that the solution behaviours displayed in Figure 10 are similar to that of the Ivlev system - see Figure 3 and Figure 5 , respectively.

By and large, the Holling II system solution behaviours for both the sub-regions of the localised structures region are similar to that of the Ivlev model. Consequently, the $2D$ model for the Holling II system is omitted for brevity.

5 | CONCLUDING REMARKS

In this paper, qualitative analysis around a coexisting steady state had been used to establish solution behaviour for a general system of nonlinear PDEs. Additionally, the necessary mathematical tools were assembled to ascertain if a localised structures region existed for the given type of PDE systems. This collection of tools incorporated both linear and weakly nonlinear analysis with an introduction of general bifurcation theory. Also, to support the selected analysis, numerical continuation and simulation processes were discussed - see Section 2.

Hence, upon the application of these mathematical tools, the central focus of this paper, was the determination of the existence of a localised structures region and the solution behaviour for two predator-prey type models with zero Neumann boundary conditions imposed on the real line. The predator-prey models that were used are typical examples of population kinetics for a predator-prey functional response. These responses being: the Ivlev (Section 3) and the ratio-dependent Holling type II (Section 4). It was confirmed that a localised structures region does exist for each of the Ivlev and Holling type II systems whereby this confirmation procedure was underpinned by numerical support.

Further, for each of these systems, a universal two parameter space bifurcation diagram was generated. Both of these diagrams are similar in nature whereby both included the codimension two point that indicates where the spatial instability bifurcation changes from being subcritical to supercritical. Stemming from the codimension two point for each of the systems, the localised structures region was born. Also, the BD transition curve is shown to have divided each of the localised regions into two sub-regions. These sub-regions are classified as either the isolated hole region or the snaking region. As a result, the utilisation of selected parameters values within the isolated hole region generated a single hole pattern with monotonic tail decay whereby the spatial eigenvalues are purely real spatial eigenvalues. Whereas, the choice of parameter values from the snaking region created localised holes patterns whereby the decaying tail is oscillatory with complex conjugates spatial eigenvalues. In particular,

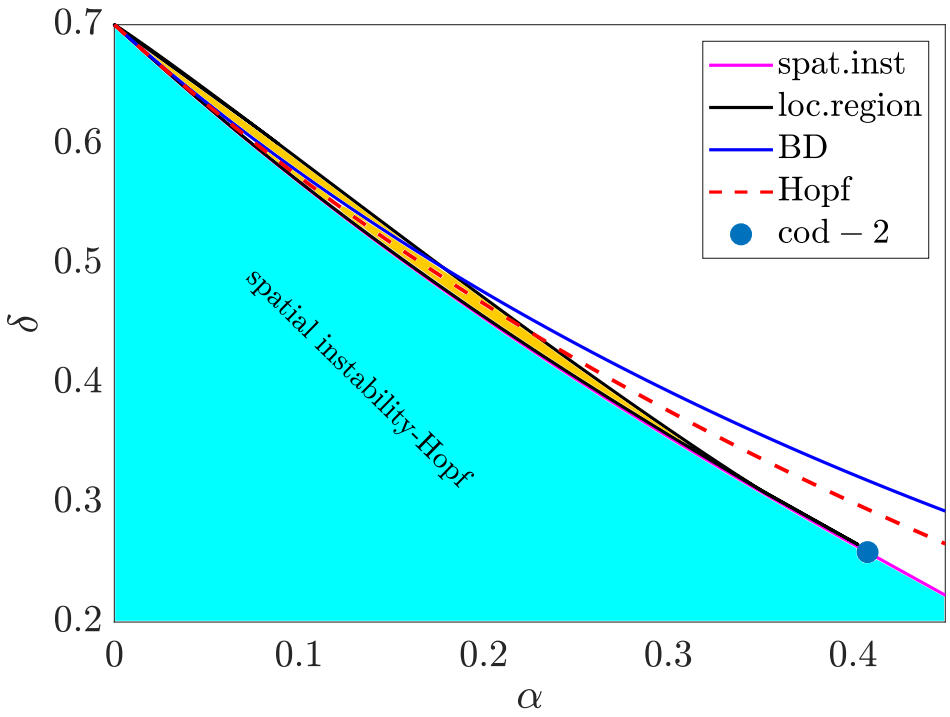

FIGURE 9 (Colour version online.) Similar bifurcation diagram to Figure 2 but for the Holling II system whereby the parameter values α, δ vary for fixed values of $\beta = 0.7$ and $\epsilon = 0.06$. The blue dot indicates where the codimension two point lies.

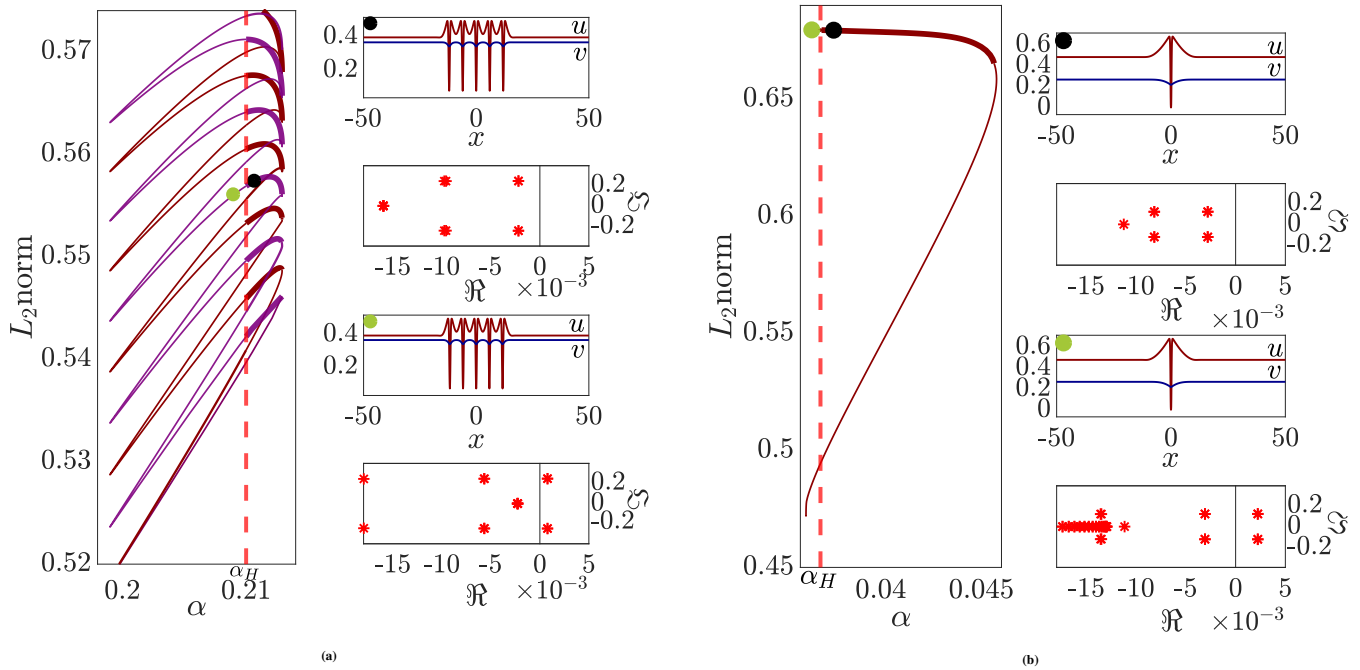

FIGURE 10 (Colour version online.) Bifurcation diagrams in the (α, L_2norm) space with solution plots for selected values of α. (a) Homoclinic snaking bifurcation for $\delta = 0.457$ as α varies. The thick (thin) line indicates stable (unstable) solutions where the purple (brown) presents that the number of holes in the solution is odd (even). Also two solutions with different stability mark by black (stable) and green (unstable) dot in the snaking bifurcation. (b) Bifurcation of one parameter continuation in the isolated hole region for $\delta = 0.65$. The insert plots show example solutions and the corresponding linear spectrum stability.

pattern formation was explored in the limit where the prey population diffuses much more slowly than that of the predator population.

As a localised structures region existed for both systems, the displayed details regarding the bifurcation diagrams were similar. For directness, the centre of attention had remained with the Ivlev system. It was noted that the Hopf bifurcation curve for the coexistent steady state cut through the localised structures region. This curve added complexity via the creation of instabilities in the localised patterns of the region. That is, temporal periodic localised patterns arose at nearby parameter values to the Hopf bifurcation curve with a stable limit cycle occurring just beyond the Hopf bifurcation. Once again this scenario was similar to the Holling II system and the details were not shown in this paper.

Finally, to determine solution behaviour for the $2D$ case, similar $1D$ parameter values were used. For brevity, only the $2D$ Ivlev system heat maps and the corresponding time series were presented. These results established that, for both systems, there was an onset of intricate spatio-temporal patterns as that for the $1D$ system.

5.1 | Bibliography

References

1. Murray JD. *Mathematical Biology II : Spatial Models and Biomedical Applications*. New York, NY: Springer New York : Imprint: Springer. third edition. ed. 2003.

2. Camara B, Aziz-Alaoui M. Complexity in a prey-predator model. *Revue Africaine de la Recherche en Informatique et Mathématiques Appliquées* 2008; 9: 109-122.

3. Berryman A. The Orgins and Evolution of Predator-Prey Theory. *Ecology* 1992; 73(5): 1530-1535.

4. Volterra V. Variations and Fluctuations of the Number of Individuals in Animal Species living together. *ICES Journal of Marine Science* 1928; 3(1): 3-51.

5. Lotka AJ. ELEMENTS OF PHYSICAL BIOLOGY. *Science Progress in the Twentieth Century (1919-1933)* 1926; 21(82): 341–343.

6. Bateman PW, Fleming PA, Wolfe AK. A different kind of ecological modelling: the use of clay model organisms to explore predator–prey interactions in vertebrates. *Journal of Zoology* 2017; 301(4): 251-262.

7. Smith JA, Suraci JP, Hunter JS, et al. Zooming in on mechanistic predator–prey ecology: Integrating camera traps with experimental methods to reveal the drivers of ecological interactions. *Journal of Animal Ecology* 2020; 89(9): 1997-2012.

8. DeLong J, Lyon S. Temperature alters the shape of predator–prey cycles through effects on underlying mechanisms. *PeerJ* 2020; 8.

9. F. Berezovskaya G, Karev BS, Castillo-Chavez C. A Simple Epidemic Model with Surprising Dynamics. *Mathematical Biosciences and Engineering* 2005; 2: 133.

10. Goodwin RM. *A Growth Cycle*: 165–170; London: Palgrave Macmillan UK . 1982.

11. Kim DH, Kim DH. A system dynamics model for a mixed-strategy game between police and driver. *System Dynamics Review* 1997; 13(1): 33-52.

12. Arecchi F, Boccaletti S, Ramazza P. Pattern formation and competition in nonlinear optics. *Physics Reports* 1999; 318(1): 1 - 83.

13. Wilczek, M. , Tewes, W. B.H. , Gurevich, S. V. , Köpf, M. H. , Chi, L. F. , Thiele, U. . Modelling Pattern Formation in Dip-Coating Experiments. *Math. Model. Nat. Phenom.* 2015; 10(4): 44-60. doi: 10.1051/mmnp/201510402

14. Dickstein AJ, Erramilli S, Goldstein RE, Jackson DP, Langer SA. Labyrinthine Pattern Formation in Magnetic Fluids. *Science* 1993; 261(5124): 1012–1015.

15. Turing AM. The chemical basis of morphogenesis. *Philosophical Transactions of the Royal Society of London. Series B, Biological Sciences* 1952; 237(641): 37-72.

16. Camara B, Aziz-Alaoui M. Dynamics of a predator-prey model with diffusion. *Dynamics of Continuous, Discrete and Impulsive Systems Series A: Mathematical Analysis* 2008; 15(6): 897-906.

17. Zhou J. Bifurcation Analysis of a Diffusive Predator–Prey Model with Bazykin Functional Response. *International Journal of Bifurcation and Chaos* 2019; 29(10): 1950136.

18. Petrovskii SV, Malchow H. Wave of Chaos: New Mechanism of Pattern Formation in Spatio-temporal Population Dynamics. *Theoretical Population Biology* 2001; 59(2): 157 - 174.

19. Wang J. Spatiotemporal Patterns of a Homogeneous Diffusive Predator–Prey System with Holling Type III Functional Response. *Journal of Dynamics and Differential Equations* 2017; 19(29): 1383-1409.

20. Wang L. Spatial pattern formation of a ratio-dependent predator prey model. *Chinese Physics B* 2010; 19(9): 090206.

21. Wang W, Zhang L, Wang H, Li Z. Pattern formation of a predator–prey system with Ivlev-type functional response. *Ecological Modelling* 2010; 221(2): 131 - 140.

22. Alonso D, Bartumeus F, Catalan J. MUTUAL INTERFERENCE BETWEEN PREDATORS CAN GIVE RISE TO TURING SPATIAL PATTERNS. *Ecology* 2002; 83(1): 28-34.

23. Knobloch E. Spatial Localization in Dissipative Systems. *Annual Review of Condensed Matter Physics* 2015; 6: 325-359.

24. Champneys A, Al Saadi F, Breña–Medina V, et al. Bistability, wave pinning and localisation in natural reaction-diffusion systems. *Physica D.* 2020. In press: Available online at urlhttps://doi.org/10.1016/j.physd.2020.132735.

25. Brena–Medina V, Champneys AR. Subcritical Turing bifurcation and the morphogenesis of localized patterns. *Phys. Rev. E* 2014; 90: 032923.

26. Gandhi P, Zelnik YR, Knobloch E. Spatially localized structures in the Gray-Scott model. *Philosophical Transactions of the Royal Society A: Mathematical, Physical and Engineering Sciences* 2018; 376(2135): 20170375.

27. Abshagen J, Heise M, Pfister G, Mullin T. Multiple localized states in centrifugally stable rotating flow. *Physics of Fluids - PHYS FLUIDS* 2010; 22.

28. Parra-Rivas P, Gomila D, Gelens L, Knobloch E. Bifurcation structure of localized states in the Lugiato-Lefever equation with anomalous dispersion. *Phys. Rev. E* 2018; 97: 042204.

29. Meron E. *Nonlinear Physics of Ecosystems*. CRC Press. 3rd ed. 2015.

30. Al Saadi F, Worthy A, Pillai JR, Msmali A. Localised structures in a virus-host model. *Journal of Mathematical Analysis and Applications* 2021; 499(1): 125014.

31. Al Saadi F, Worthy A, Msmali A, Champneys A. Stationary and oscillatory localized patterns in ratio-dependent predator-prey systems. 2020. Preprint, University of Bristol.

32. Al Saadi F, Champneys A, Verschueren N. Localised patterns and semi-strong interaction, a unifying framework for reaction-diffusion systems.. 2020. In preparation.

33. Cross M, Hohenberg P. Pattern formation outside of equilibrium. *Rev. Mod. Phys.* 1993; 65: 851–1112.

34. Champneys A. Homoclinic orbits in reversible systems and their applications in mechanics, fluids and optics. *Physica D: Nonlinear Phenomena* 1998; 112(1): 158 - 186.

35. Haragus M, Iooss G. *Local Bifurcations, Center Manifolds and Normal Forms in Infinite Dimensional Dynamical Systems*. New York: Springer . 2007.

36. Devaney RL. Reversible Diffeomorphisms and Flows. *Transactions of the American Mathematical Society* 1976; 218: 89–113.

37. Verschueren N, Champneys A. A Model for Cell Polarization Without Mass Conservation. *SIAM Journal on Applied Dynamical Systems* 2017; 16(4): 1797-1830. doi: 10.1137/16M1093847

38. Holling CS. The Components of Predation as Revealed by a Study of Small-Mammal Predation of the European Pine Sawfly. *The Canadian Entomologist* 1959; 91(5): 293–320. doi: 10.4039/Ent91293-5

39. Ivlev V. *Experimental Ecology of the Feeding of Fishes*. Yale University Press . 1961.

40. Rosenzweig ML. Paradox of Enrichment: Destabilization of Exploitation Ecosystems in Ecological Time. *Science* 1971; 171(3969): 385–387.

41. May RM. Limit Cycles in Predator-Prey Communities. *Science* 1972; 177(4052): 900–902.

42. Hwang TW. Uniqueness of limit cycles of the predator–prey system with Beddington–DeAngelis functional response. *Journal of Mathematical Analysis and Applications* 2004; 290(1): 113 - 122.

43. Cheng KS, Hsu SB, Lin SS. Some results on global stability of a predator-prey system. *Journal of Mathematical Biology* 1982; 12: 115-126.

44. Kooij R, Zegeling A. A Predator–Prey Model with Ivlev's Functional Response. *Journal of Mathematical Analysis and Applications* 1996; 198(2): 473 - 489.

45. Wang X, Wei J. Dynamics in a diffusive predator–prey system with strong Allee effect and Ivlev-type functional response. *Journal of Mathematical Analysis and Applications* 2015; 422(2): 1447 - 1462.

46. Wang X, Wei J. Diffusion-driven stability and bifurcation in a predator–prey system with Ivlev-type functional response. *Applicable Analysis* 2013; 92(4): 752-775.

47. Gazi NH. Dynamics of a marine plankton system: Diffusive instability and pattern formation. *Applied Mathematics and Computation* 2012; 218(17): 8895 - 8905.

48. Pearce I, M.A.J. C, Peter G. Schofield P, Anderson A, Hubbard S. Modelling the spatio-temporal dynamics of multi-species host–parasitoid interactions: Heterogeneous patterns and ecological implications. *Journal of Theoretical Biology* 2006; 241(4): 876 - 886.

49. Liu B, Zhi Y, Chen LS. The dynamics of a predator-prey model with Ivlev's functional response concerning integrated pest management. *Acta Mathematicae Applicatae Sinica* 2004; 20(1): 133-146.

50. Metz JAJ, Diekmann O. A Gentle Introduction to Structured Population Models: Three Worked Examples. In: Springer Berlin Heidelberg; 1986; Berlin, Heidelberg: 3–45.

51. Sherratt J, Eagan B, Lewis M. Oscillations and chaos behind predator prey invasion: mathematical artifact or ecological reality?. *Philosophical Transactions of the Royal Society of London. Series B: Biological Sciences* 1997; 352(1349): 21-38.

52. Ling L, Wang W. Dynamics of a Ivlev-type predator–prey system with constant rate harvesting. *Chaos, Solitons & Fractals* 2009; 41(4): 2139 - 2153.

53. Zhang Cq, Liu L, Yan P, Zhang Lz. Stability and Hopf bifurcation analysis of a predator-prey model with time delayed incomplete trophic transfer. *Acta Math. Appl. Sin. Engl. Ser. 31* 2015: 235 - 246.

54. Baek H, Kim S, Kim P. Permanence and stability of an Ivlev-type predator–prey system with impulsive control strategies. *Mathematical and Computer Modelling* 2009; 50(9): 1385 - 1393.

55. Xiang Z, Song X. The dynamical behaviors of a food chain model with impulsive effect and Ivlev functional response. *Chaos, Solitons & Fractals* 2009; 39(5): 2282 - 2293.

56. Woods P, Champneys A. Heteroclinic tangles and homoclinic snaking in the unfolding of a degenerate reversible Hamiltonian-Hopf bifurcation. *Phys. D* 1999; 129: 170-174.

57. M. B, Knobloch J, Lloyd D, Sandstede B, Wagenknecht T. Snakes, ladders,and isolas of localized patterns. *SIAM J. Math. Anal.* 2009; 41: 936-972.

58. Baurmann M, Gross T, Feudel U. Instabilities in spatially extended predator–prey systems: Spatio-temporal patterns in the neighborhood of Turing–Hopf bifurcations. *Journal of Theoretical Biology* 2007; 245(2): 220 - 229.

59. Hu G, Li X, Wang Y. Pattern formation and spatiotemporal chaos in a reaction–diffusion predator–prey system. *Nonlinear Dynamics* 2015; 81: 265–275.

60. Holling CS. The functional response of invertebrate predators to prey density. *Memoirs of the Entomological Society of Canada* 1966; 98: 5-86.

61. Zhou J, Mu C. Coexistence states of a Holling type-II predator–prey system. *Journal of Mathematical Analysis and Applications* 2010; 369(2): 555 - 563.

62. Yin H, Wen X. Pattern Formation through Temporal Fractional Derivatives. *Scientific reports* 2018; 8: 5070.

63. Cheng KS. Uniqueness of a Limit Cycle for a Predator-Prey System. *SIAM Journal on Mathematical Analysis* 1981; 12(4): 541-548.

64. Hsu SB, Shi J. Relaxation oscillation profile of limit cycle in predator-prey system. *Discrete and Continuous Dynamical Systems-B* 2009; 11: 893.

65. Bie Q, Wang Q, Yao aZ. Cross-diffusion induced instability and pattern formation for a Holling type-II predator–prey model. *Applied Mathematics and Computation* 2014; 247: 1 - 12.

66. Michaelis L, Menten ML. Die kinetik der invertinwirkung. *Biochem. z* 1913; 49(333-369): 352.